Published in final edited form as:
Biochemistry. 2009 June 16; 48(23): 5121–5130. doi:10.1021/bi9001387.

Redox dependent conformational changes in cytochrome *c* oxidase suggest a gating mechanism for proton uptake[†,‡]

Ling Qin[§], **Jian Liu**, **Denise A. Mills**, **Denis A. Proshlyakov**, **Carrie Hiser**, and **Shelagh Ferguson-Miller**[*]
Biochemistry and Molecular Biology Department, Michigan State University, East Lansing, MI 48824

Abstract

A role for conformational change in the coupling mechanism of cytochrome *c* oxidase is the subject of controversy. Relatively small conformational changes have been reported in comparisons of reduced and oxidized crystal structures of bovine oxidase, but none in bacterial oxidases. Comparing the x-ray crystal structures of the reduced (at 2.15 Å resolution) and oxidized forms of cytochrome *c* oxidase from *Rhodobacter sphaeroides*, we observe a displacement of heme a_3 involving both the porphyrin ring and the hydroxyl farnesyl tail, accompanied by protein movements in nearby regions, including the mid part of helix VIII of subunit I which harbors key residues of the K proton uptake path, K362 and T359. The conformational changes in the reduced form are reversible upon reoxidation. They result in an opening of the top of the K pathway and more ordered waters being resolved in that region, suggesting an access path for protons into the active site. In all high resolution structures of oxidized *Rhodobacter sphaeroides* cytochrome *c* oxidase, a water molecule is observed in the hydrophobic region above the top of the D path, strategically positioned to facilitate the connection of residue E286 of subunit I to the active site or to the proton pumping exit path. In the reduced and reduced plus cyanide structures, this water molecule disappears, implying disruption of proton conduction from the D path under conditions when the K path is open, thus providing a mechanism for alternating access to the active site.

Cytochrome *c* oxidase (C*c*O)[1], the terminal enzyme of the electron transfer chain, provides the final electron sink by accepting electrons from reduced cytochrome *c* and passing them sequentially through Cu_A, heme *a* and finally to its active site, composed of heme a_3 and Cu_B. Oxygen binds at this binuclear center, accepts the electrons and is reduced to water. The energy released from oxygen reduction is utilized by C*c*O to translocate protons from the N (negative)-side of the membrane to the P(positive)-side, to generate an transmembrane proton electrochemical gradient, which is then used for ATP synthesis (for recent reviews, see ref. ([1–3])). Extensive kinetic and spectroscopic studies have identified intermediate states during the chemical catalysis, yet the details of the oxygen reduction process are not entirely understood. Even more elusive and controversial is the proton pumping mechanism.

[†]This work is supported by National Institutes of Health Grant GM26916 (S.F.-M.) and GM070544 (D.A.P.), Michigan State University Research Excellence Fund Grant 03-016 (S.F.-M.), and Michigan Technology Tri-Corridor Center for Structural Biology Core Technology Alliance Grant 085P1000817.

[‡]The atomic coordinates and structure factors of reduced and cyanide-bound reduced *Rhodobacter sphaeroides* cytochrome *c* oxidase have been deposited in the Protein Data Bank with access codes of 3FYE and 3FYI, respectively.

[*]To whom correspondence should be addressed: Phone: 517-355-0199; Fax: 517-353-9334; E-mail: E-mail: fergus20@msu.edu.
[§]Present address: Department of Biomass Science and Conversion Technology, Sandia National Laboratories, Livermore, CA 94551

Supporting Information Available: Schematic drawing of the microspectrophotometer used for spectral analysis of single crystal (Figure S1), comparison of the distances between heme a_3 farnesyl-OH and Y288$_I$-OH, as well as the distances between Cu_B and heme a_3 Fe in different forms of *Rs*C*c*O (Table SI). This materials is available free of charge via the Internet at http://pubs.acs.org.

Two types of protons, termed pump and substrate protons, are taken up from the N-side of the membrane. During each catalytic cycle, four pump protons are translocated to the P-side of the membrane, while four substrate protons are used in the oxygen reduction to water. Previous studies on bacterial C*c*O have identified two proton uptake pathways, D and K, within the transmembrane portion of the enzyme ([4, 5]). They are named after key residues in each pathway, $D132_I$ and $K362_I$ (*Rhodobacter sphaeroides* (*Rs*) C*c*O numbering, with the subscript representing the subunit), respectively. These two pathways contain crystallographically resolved water molecules which, together with polar residues, enable proton conduction ([4, 6, 7]).

The D path is considered to transport all of the pump protons, as well as at least two substrate protons ([8, 9]). In the high resolution crystal structures of *Rs*C*c*O, a clear chain of hydrogen bonded water molecules are resolved in the vicinity of the D pathway, between $D132_I$ and $E286_I$ ([6, 7]). The latter residue is considered to be the branching point beyond which a proton is either translocated to the outside of the membrane via an unidentified route, or transported to the binuclear center for oxygen reduction to water ([10, 11]).

Evidence suggests that the K path is used for transporting one to two substrate protons during the reductive half of the oxygen chemistry cycle (O→R) ([12, 13]). The path is considered to start with E101 of subunit II ([14]) (but see ref ([15])), and involve key residues $S299_I$, $K362_I$ and $T359_I$, the latter two located in the middle part of helix VIII of subunit I. The mutation of these residues leads to a major loss of activity, up to 99.95% for K362M ([5, 16]). Compared with the D path, there are very few water molecules resolved, only two in the available crystal structures so far. One is hydrogen bonded to $K362_I$ and $S299_I$, the other to $T359_I$ and the OH group of heme a_3 hydroxylfarnesyl tail (heme a_3 farnesyl-OH) ([6, 7]). The latter group also forms a strong hydrogen bond with the OH group of $Y288_I$ ($Y288_I$-OH), which has a unique covalent bond between the side chain atoms with the Cu_B ligand $H284_I$ in the active site. The strong hydrogen bonding between $Y288_I$-OH and heme a_3 farnesyl-OH (O – O distance of 2.6 Å) is proposed to function as a closed K path gate, since its presence prohibits proton transport via that path to the active site ([17, 18]). This fits with the hypothesis that in the oxidized state, the K-path is expected to be closed ([19]). No water molecules are resolved between $Y288_I$ and the binuclear center in all the oxidized C*c*O crystal structures, even at high resolution.

In this communication, we report the structure of the dithionite reduced form of *Rs*C*c*O, a bacterial enzyme highly homologous to the mammalian mitochondrial C*c*O. The structure shows a significant displacement of heme a_3, leading to the loss of the strong hydrogen bond between Y288-OH and heme a_3 farnesyl-OH, the movement of the middle part of helix VIII that contains key residues of the K path, and appearance of resolved water molecules leading from the top of the K path into the binuclear center. These observed changes, along with the loss of a water molecule above the D path, suggest conformational control of alternate opening of the K and D paths for proton transport to the active site.

MATERIALS AND METHODS

Protein expression, purification and crystallization of RsCcO

In order to obtain I-II *Rs*C*c*O crystals, *Rs* cells (strain 37Δ4 ([7])) were grown and harvested, and membrane samples prepared as described ([20]). The protein purification and crystallization procedure were described earlier ([7]). In order to obtain four subunit *Rs*C*c*O crystals, *Rs* strain 169 was generated by transferring plasmid pCH169 ([7]) into *Rs* strain YZ200 ([20]). The growth and harvest of the cells and preparation of plasma membranes were described earlier ([20]). The protein purification and crystallization procedure for four subunit *Rs*C*c*O were described earlier ([21]).

Treatments of RsCcO crystals to produce the reduced form and the cyanide bound reduced form

Prior to flashcooling, crystals of *Rs*C*c*O were soaked in a stabilizing solution containing 91 mM MES, pH 6.3, 18.2 mM Tris, pH 8.0, 91 mM NaCl, 30 mM $MgCl_2$, 2 mM $CdCl_2$, 0.16% decyl maltoside, 0.013% dodecyl maltoside, 4.4% 1,2,3-heptanetriol, 24% (v/v) PEG-400, and supplemented with 10mM sodium dithionite. The crystals were soaked for 5 – 10 minutes at 4°C to reduce the crystals. The C*c*O crystals turned green within a few minutes and remained green throughout the entire process. The surrounding solution was gradually exchanged into the cryosolution that contained the same ingredients as in the stabilizing solution except for a higher concentration (32%) of PEG-400, also supplemented with 10 mM sodium dithionite. The crystals were then picked and flashcooled in liquid nitrogen.

To produce cyanide bound reduced *Rs*C*c*O crystals, the crystals were first reduced as described above by adding stabilizing solution supplemented with 10 mM dithionite. The surrounding stabilizing solution was then exchanged into a new stabilizing solution supplemented with 10 mM dithionite and 20 mM cyanide. The crystals were soaked in this solution for another 5 minutes. The surrounding solution was then gradually exchanged into cryosolution with 32% PEG-400, also supplemented with 10 mM dithionite and 20 mM cyanide. The cyanide bound reduced crystals were then flashcooled in liquid nitrogen.

Removal of Cd from I-II RsCcO Crystals

Crystals of I-II *Rs*C*c*O were soaked in stabilizing solution as described earlier, except that no Cd was present, for 1 hour. The soaking solution was then exchanged into a fresh stabilizing solution containing 10 mM dithionite, still without Cd, for another 45 minutes. The stabilizing solution was then slowly exchanged into the Cd-free cryosolution supplemented with dithionite as described earlier, prior to flashcooling in liquid nitrogen.

Reoxidation of reduced RsCcO crystal

Crystals of I-II *Rs*C*c*O were reduced with 10 mM dithionite as described above. The soaking solution was then exchanged into a stabilizing solution with no dithionite. The soaking solution free of dithionite was then slowly exchanged into cryosolution containing 32% PEG-400, with no dithionite and supplemented with 1 mM ferricyanide. The crystals turned from green to brownish red during the exchanging process, which took approximately 5 minutes. The re-oxidized crystals were soaked in the cryosolution with ferricyanide for another 5 minutes prior to being flashcooled in liquid nitrogen.

X-ray crystallographic data collection and structural refinement

X-ray diffraction data of the dithionite reduced, as well as Cd-free reduced, I-II *Rs*C*c*O crystals, were collected at Station 23-ID-B, GM/CA-CAT, Advanced Photon Source, Argonne National Laboratory. Diffraction data from the cyanide bound reduced form, as well as the reduced/reoxidized form of I-II *Rs*C*c*O crystals were collected at Station 21-ID-G, LS-CAT, Advanced Photon Source, Argonne National Laboratory. The data were processed with HKL2000 ([22]), and the structures were solved by molecular replacement using the oxidized I-II subunit *Rs*C*c*O (PDB entry 2GSM ([7])) as the starting model, and refined by Refmac5 ([23]) from the CCP4 program suite ([24]). Molecular visualization and model building were performed using the program COOT ([25]). The refinement statistics for the final models of reduced and cyanide-bound reduced I-II *Rs*C*c*O are presented in Table 1. All figures with molecular models were generated using the program PYMOL (DeLano Scientific, CA).

The diffraction data for reduced four subunit *Rs*C*c*O crystal were collected at station 21-ID-D, LS-CAT, Advanced Photon Source, Argonne National Laboratory. The crystal diffracted

anisotropically to approximately 3.2 Å resolution. The structure was determined by molecular replacement using the published oxidized four subunit *Rs*C*c*O structure (PDB entry 1M56([6])) as the starting model and refined using CNS1.1 ([26]).

In order to confirm the loss of Cd at the $E101_{II}$ site for the Cd-free reduced I-II *Rs*C*c*O crystal, anomalous diffraction data were collected at station 23-ID-B, GM/CA-CAT, Advanced Photon Source, Argonne National Laboratory. The wavelength of the X-ray was set at 1.984 Å, where cadmium has a strong anomalous signal. The published oxidized two subunit *Rs*C*c*O structure (PDB entry 2GSM ([7])) was used as the starting phasing model in a rigid body refinement, and the anomalous difference Fourier map was calculated with the CCP4 program suite ([24]) using the phases of the rigid-body refined structure. In order to minimize bias, all metals in the structure were removed from the phase calculation.

Spectral studies of irradiated reduced RsCcO crystals

Optical absorption measurements in crystals were carried out using a fiber optics spectrometer (model S2000, Ocean Optics, USA). One end of a 50 μm optical fiber was attached to the spectrometer while the other end was fixed pointing upward (for detailed setup, see Figure S1 of the supporting materials). A short length of tubing was placed over the fiber termination ferrule (3.2 mm diam.) forming a sample dish ~1 mm deep. Transmission light was provided by tungsten lamp, which was offset from the optical fiber axis by 40° at a distance of approx. 50 cm. A paper diffuser (10 cm diam.) located 2 cm above the sample dish provided a uniform, broad-angle light illumination source. Only the light scattered by the diffuser, but not the direct light from the lamp, could be collected by the 25° (in the air) acceptance angle of the optical fiber. No other light sources were present. The sample dish was filled with the cryoprotectant buffer for reference measurements (150 sec). While the diffuser was removed, a previously reduced and irradiated crystal from liquid nitrogen was placed in the buffer and a microscope was used to position the crystal directly above the optical fiber. Sample measurements were started immediately after repositioning the diffuser and spectra were recorded continuously every 0.2 sec and averaged in 30 sec intervals throughout the experiment. Configuration with a diffuse probe light showed little sensitivity to the loss of light due to refractivity and scattering on crystal surfaces and protein aggregates.

On-line single-crystal micro-spectroscopy

The on-line single-crystal micro-spectrophotometer available at station 14-BM-C, BioCARS, Advanced Photon Source, Argonne National Laboratory was used to record the spectrum of CN-bound reduced I-II *Rs*C*c*O frozen crystal. The assembly of the equipment is described in detail elsewhere ([27]). Due to the anisotropic arrangements of chromophores in protein crystals, which can lead to large spectral distortion depending upon the crystal orientation, the crystal was carefully aligned so that the resulting spectrum resembles the isotropic solution spectrum.

Oxidase Activity Assay

Measurements of the rates of O_2 reduction were performed at 25°C using an oxygen electrode. For assay at pH 6.2, the reaction mixture (total volume 1.8 ml) contained 50 mM MES-KOH, pH 6.2, 19 mM KCl, 2.8 mM ascorbate, 1.1 mM TMPD, 0.1% dodecyl maltoside, 6.7 nM C*c*O, and 30 μM horse heart cytochrome *c*. For assay at pH 7.4, the reaction mixture contained 50 mM HEPES, pH 7.4, 24 mM KCl, 2.8 mM ascorbate, 1.1 mM TMPD, 0.1% dodecyl maltoside, 6.7 nM C*c*O, and 30 μM horse heart cytochrome *c*.

RESULTS

Displacement of heme a_3 in the reduced RsCcO structure

The crystal structure of the dithionite reduced *Rs*C*c*O was determined at 2.15 Å resolution (see Table 1 for data collection and refinement statistics). The reduced *Rs*C*c*O shows no significant conformational changes in the overall structure of the enzyme except in regions near the active site, most notably in the heme a_3 moiety. In comparison to the oxidized structure (PDB entry 2GSM) ([7]), the heme a_3 porphyrin ring rotates 6–8° about the carboxyl group of the A-ring propionate, as seen from the direction of Cu_B (Figure 1(A) and (B)). This rotation is accompanied by a subtle tilt of the plane of the porphyrin ring. The continuous electron density between the two metals of the binuclear center in the oxidized structure (Figure 2(A)), tentatively assigned to be a water and a OH^- bound to Fe-a_3 and Cu_B, respectively ([7]), is gone. The absence of the bridging ligands was also observed in the reduced C*c*O structures from *Paracoccus denitrificans* (*Pd*) ([28]), bovine ([29]), and *Thermus thermophilus* ([30]). Therefore, it appears that in the fully reduced state (R state), the two product water molecules are no longer bound to the binuclear center metals, consistent with results from the resonance Raman spectroscopic studies which show the Fe-a_3 is five coordinated in the reduced state ([31]). Due to the missing bridging ligands in the binuclear center, the Fe^{2+} atom is more out of the plane of the porphyrin ring, moved toward the $His419_I$ ligand, and the distance between Fe^{2+}–a_3 and Cu^{1+}_B becomes larger (5.4 Å in the reduced state compared to 4.9 Å in the oxidized state) (Figure 2(B)) (Table S1 of the supporting information). Besides the movement of the porphyrin ring, the hydroxylfarnesyl tail undergoes significant rotational movement, which widens the distance between the heme a_3 farnesyl -OH and $Y288_I$-OH from a tight hydrogen bonding distance of 2.6 Å in the oxidized structure (Figure 2(A)) to approximately 4.1 Å in the reduced (Figure 2(B))(Table S1 of the supporting information).

Moreover, compared with the oxidized structure (Figure 2(A)), there are four more water molecules clearly resolved in the region, including one that sits between the now separated $Y288_I$-OH and heme a_3 farnesyl-OH, as shown in Figure 2(B). These additional water molecules provide a hydrogen bonded water chain, connecting the upper part of the K path to the binuclear center.

Movements in the protein in the reduced RsCcO structure

The conformational change in heme a_3 is accompanied by significant movement of the protein in nearby regions, especially the mid part of helix VIII (shown in Figure 1(A)), involving residues 355–364 of subunit I (Figure 1(A) and (B)). On the distal side of the heme a_3 plane, in the angle between the porphyrin rings of heme *a* and a_3, additional movement of the protein is observed involving residues 423–426 of helix X (Figure 1(B)). The conformational change of $S425_I$ is the most striking: not only is the main chain C-α atom moved 2.9Å in the reduced structure, its side-chain OH group points in the opposite direction from that in the oxidized form. Similar movements in these residues were also seen in the reduced bovine C*c*O structure (see Discussion). Not seen in the bovine C*c*O, a few residues on the other side of heme a_3 are moved, in helix IX of *Rs*C*c*O centered on $Ile399_I$, accommodating the heme a_3 ring and tail displacement towards them.

Structure of the cyanide-bound reduced RsCcO

Cyanide binds at the active site of cytochrome oxidase and prevents oxygen binding, hence its potent toxic effect on cellular metabolism ([32]). The structure of the CN-bound, reduced *Rs*C*c*O was solved at 2.2 Å resolution (see Table 1 for data collection and structural refinement statistics). The binding of CN to reduced *Rs*C*c*O was confirmed by the absorption spectrum of the frozen crystal before x-ray irradiation (Figure 3), obtained at station 14-BM-C, BioCARS, Advanced Photon Source, Argonne National Laboratory, using their custom-built on-line

single-crystal microspectrometer setup as described ([27]). The spectrum shows the expected broadened α peak in the 590–606 region ([33]) (in contrast to the reduced C*c*O spectrum, Figure 6) . Compared with the reduced active site with no bridging ligand (Figure 2(B), the CN molecule was clearly resolved between the two metals, shown in Figure 2(C). It is noteworthy that although previous studies on bovine C*c*O have suggested two CN binding interactions at the binuclear center ([34]), our crystal structure of CN-bound *Rs*C*c*O only reveals one binding geometry, likely representing only the predominant form under our experimental conditions. The same displacement of the porphyrin ring of heme a_3, together with the movement of the mid part of helix VIII seen in reduced structure without CN, is also observed in the CN-bound, reduced structure. However, due to strong interaction between the carbon ion of CN and Fe-a_3, the Fe^{2+} has moved back towards the plane of the porphyrin ring and the distance between Cu_B and Fe-a_3 is approximately 5.0 Å, similar to that in the oxidized structure. Moreover, there are only three, rather than four, additional waters resolved between the top of the K path and the active site, with the one closest to the active site missing (Figure 2(B) and (C)).

Structure of the D pathway in the reduced state

In contrast to the structure of the K path, there are no major protein conformational changes observed in the D path in the reduced vs. oxidized state. As shown in Figure 4, there is no difference in the ordered, hydrogen-bonded water network connecting the vicinity of $D132_I$ to the vicinity of $E286_I$, or in the aligning residues. The only significant change in the D path region between the reduced and oxidized structure is in the hydrophobic area between $E286_I$ and the active site. In the oxidized structure, there is a water molecule (W301) resolved in this location. This water disappears in the reduced structure and in the reduced CN-bound form. The potential significance of this change is further elaborated later (see Discussion).

Structure of reduced RsCcO with no Cd bound to $E101_{II}$ at K path entrance

Cadmium is an essential ingredient in our crystallization experiments because it mediates intermolecular crystal contacts ([7]). Similar to Zn, it is also an known inhibitor of C*c*O ([35, 36]). One of the inhibitory binding sites is at the entrance of the K path, $E101_{II}$ ([21]). In fact, cadmium is found bound to $E101_{II}$ and $H96_{II}$ in our I-II subunit *Rs*C*c*O structures in both oxidized and reduced forms. It is conceivable that the structural changes observed in this work are somehow related to the fact that the enzyme is inhibited in the K path during dithionite reduction. In order to test this possibility, a number of crystals were soaked in a Cd-free stabilizing solution for different periods of time, followed by dithionite reduction. The data collection on these crystals was performed at the selected wavelength of 1.974 Å (6250 eV) where Cd has a strong anomalous signal, and the presence of Cd at the $E101_{II}$ site was checked by an anomalous difference Fourier map. Soaking in Cd-free solution led to Cd dissociation both at the $E101_{II}$ site and at the crystal contact region; the diffraction limit of these reduced crystals deteriorated significantly to only 3.3 Å. Nevertheless, it was found that a 1-hour soaking in Cd-free stabilizing solution followed by a 45-minutes soaking with stabilizing solution supplemented with dithionite, completely removed the Cd binding at the $E101_{II}$ site, as evidenced by the disappearance of the intense peak in the anomalous difference Fourier map. The C*c*O crystal structure with no Cd at $E101_{II}$ site still showed the displacement of heme a_3 and regions in helix VIII, as described earlier. Due to the lower diffraction resolution limit, we were unable to confirm the presence of the additional water molecules between $T359_I$ and the binuclear center; however, it is reasonable to conclude that the conformational changes we see in this study are not a result of the inhibitory binding of Cd at $E101_{II}$ site.

This conclusion is reinforced by studies with the 4-subunit crystal that is produced in the absence of Cd. This crystal form diffracts to lower resolution than the two-subunit enzyme crystal; the reduced state was solved at a resolution of 3.2 Å. Although the structure is not of the resolution to reveal all atomic details, it still clearly shows the key findings of this work,

including the displacement of heme a_3, as evidenced by the widening of the distance between $Y288_I$-OH and heme a_3 farnesyl-OH (Table S1 of the supporting information), as well as the main chain movement of the mid part of helix VIII. The result confirms that neither the presence of Cd, nor the absence of subunit III is responsible for the observed conformational changes.

Reversibility of the conformational changes in reduced RsCcO

In order to test whether the conformational changes in the reduced structure were reversible, a reduced I-II *Rs*C*c*O crystal was subject to reoxidation by ferricyanide, and the structure of the reoxidized crystal was determined. The reduced, then reoxidized structure is essentially the same as that of the oxidized, with all the conformational changes in the heme a_3 group, as well as in the protein moiety returned to the oxidized state (Table S1 of the supporting information).

Biochemical characterization of redissolved, reduced I-II RsCcO crystals

The redissolved reduced crystals of I-II *Rs*C*c*O have a normal UV-Visible spectrum, as shown in Figure 5(A), as well as normal oxidase activity measured using an oxygen electrode, as shown in Figure 5(B). The redissolved reduced I-II *Rs*C*c*O crystals show suicide inactivation, typical for C*c*O lacking subunit III ([37]), which can be rescued by lower pH ([37]) (Figure 5(B)). This effect is also seen in the redissolved oxidized crystals ([7]). The results show that no irreversible structural change has been caused by the conditions of crystallization or reduction.

Spectral characterization of RsCcO crystals after x-ray irradiation

It is well known that exposure to x-ray irradiation can have damaging effects on crystals. In the case of metalloproteins, there are additional concerns about maintenance of the redox state of the original crystal ([27]). By using a microspectrophotometer, we were able to investigate the spectral properties of single, reduced *Rs*C*c*O crystals after irradiation and the results are shown in Figure 6. (Note that due to the optical density of the crystals, the Soret peak could not be reliably recorded in all the spectral studies, and all the spectra are presented in the range of 465–850nm.) A normal reduced C*c*O spectrum was observed for crystals after data collection. Moreover, given time and fresh oxygenated soaking solution, the reduced crystal reoxidized and displayed a normal oxidized C*c*O spectrum.

DISCUSSION

It is still a major question in the field of cytochrome oxidase as to the mechanism of coupling of proton translocation to electron transport. A role for short or long range conformational changes has been proposed, linking the oxygen chemistry and redox changes in the metal centers to pK changes in proton transfer or loading sites, and altered proton conducting water pathways ([8, 18, 38–41]). Trapping intermediates in catalytic reactions is difficult crystallographically, given the tendency of crystallization to favor the most stable conformation. Yet redox-dependent protein conformational changes have been directly observed in many heme proteins. In the classic example of hemoglobin, binding of oxygen to the reduced form, or allosteric effectors, elicits long range changes in neighboring subunits ([42]). In bacterial nitrite reductase (cytochrome cd_1), the reduction of the active site heme d_1 leads to significant domain movement of the protein, as well as displacements of the heme *c* and heme d_1 groups ([43]). It is certainly the case that redox energy can be harnessed by protein conformational changes for chemical catalysis ([44]).

Redox –dependent conformational changes have also been observed in C*c*O. In the bovine mitochondrial C*c*O structure, unlike the *Rs*C*c*O, a change in position of Asp51 (bovine numbering; not conserved in *Rs*) was noted, along with rotation of the OH group of the hydroxyl farnesyl tail of the low spin heme *a* some 110° away from its original hydrogen bonding partner, $Ser382_I$ (bovine numbering; *Rs*, $Ser425_I$). This altered position is accompanied by a

conformational change in a small patch of residues involving 380–382 (bovine numbering; *Rs*, 423–425) of subunit I ([45]). The movement of this latter patch of residues was also observed in the reduced structure of *Rs*C*c*O, as shown in Figure 1. However, the hydrogen bond between heme *a* farnesyl-OH and $S382_I$-OH that is broken in bovine C*c*O is not present in the *Rs*C*c*O oxidized structure, due to a different orientation of the heme *a* farnesyl tail that is not affected by the redox state.

Heme *a*, and its precursor heme *o*, both have long hydroxyl farnesyl tails, and are always found in the active site of A-type heme copper terminal oxidases, such as the aa_3 and bo_3 oxidases. Therefore, it is likely that hemes *A* and *O* serve more purposes than merely binding the Fe ion to facilitate electron transfer, given the extra synthetic investment. One possible functional role could be to transmit conformational changes driven by the reduction of the Fe ion in the porphyrin ring, to extend its impact to nearby residues and facilitate proton transfer. Indeed, in two bacterial quinol oxidases, replacement of high spin heme *a* or heme *o* with heme *b* lead to loss of enzymatic activity ([46, 47]), while similar replacement of the low spin heme apparently yields a functional enzyme ([48]).

Differences between the reduced RsCcO structure and other reduced oxidases

The major redox-dependent changes we observed here, the displacement of heme a_3, the movement of nearby residues in helix VIII, and the new water molecules resolved between $T359_I$ and the binuclear center, have not been reported previously in C*c*O structures from other sources, including the bovine aa_3 oxidase ([29, 38]), the *P. denitrificans* aa_3 oxidase ([28]), and the thermophilic bacterial ba_3 oxidase ([30]). Although the structure of the closely related bacterial aa_3 oxidase from *Pd* in the reduced state was reported to have no corresponding changes ([28]), the coordinates are not available in the PDB for direct comparison.

In the reduced bovine C*c*O structure, the distinctive redox dependent conformational changes in residue D51 of subunit I (bovine numbering) and in the region of heme *a* led to a proposed new proton path (H path), and to a proton pumping mechanism that is centered on heme *a* and bypasses the heme-copper binuclear center ([29, 38]). This mechanism has been supported by mutational analysis in mammalian cells ([49]), but neither mutagenesis studies with bacterial C*c*Os ([50]) nor the conformational changes reported here, support the proposed bovine mechanism. The bovine and bacterial aa_3 type C*c*O share considerable sequence and structural homology, suggesting, but by no means proving, a similar mechanism for proton pumping. More studies will be required to understand the similarities and differences between these intricate energy conserving machines.

It is important to recognize that changes in crystal structures, or lack thereof, may be misleading since different conditions of crystallization may mask or favor certain conformational states. In either case, the true nature or extent of structural change may not be revealed. In this regard, the crystallization and reduction of bovine C*c*O crystals were performed at 4°C, while bovine C*c*O is designed to work at a cow's body temperature of 40°C. On the other hand, *Rs*C*c*O is designed to function well over a broader temperature range (10°C to 40°C). Studies with enzymes from the thermophilic bacteria show that there is a significant difference in their conformational flexibility at suboptimal temperatures compared to orthologous proteins from mesophilic organisms ([51]). In crystallography, the temperature is usually low and the ionic strength high, conditions that may favor a "ground state" conformation rather than a transient intermediate. This has been documented in the case of reduced and oxidized cytochrome *c* ([52, 53]).

The changes observed in our study are not seen in reduced structures of the ba_3 oxidase from *Thermus thermophilis* ([30]). Aside from the likely difference in flexibility due to a 70°C temperature optimum, this enzyme has been reported to lack a D path ([54]). If so, the mechanism

and regulation of proton uptake may be different from that of the A-type oxidase, and may not involve similar conformational changes.

The route of proton uptake through the K path

Previous studies indicate that the K path is responsible for the transport of one to two protons to the binuclear center during the initial metal reduction half of the catalytic cycle (O→R) ([8, 12, 55]). During the oxygen reduction phase of the cycle, the K path is expected to be closed ([19]) since evidence suggests that the D path alone is providing the protons during the P→F→O reactions ([8, 9, 56]). A conformational change of the $K362_I$ residue was proposed to break the hydrogen bonded network that transports protons to the active site when oxygen binds at the reduced binuclear center ([12]). Although only two water molecules, bonded to $K362_I$ and to $T359_I$, are resolved in the K path ([6, 7]), computational MD analysis predicts the presence of more water in this channel, with the ability to form a hydrogen bonded network ([57]).

In a molecular dynamics study of *Rs*C*c*O in the reduced state, a rotation of $T359_I$ was necessary to facilitate the formation of a hydrogen bonded water chain from the $K362_I$–$S299_I$ region to heme a_3 farnesyl-OH ([57]). Interestingly, a bridging water molecule was also observed for an extended period of time between $Y288_I$-OH and heme a_3 farnesyl-OH, as observed in this study. Additional fixed water molecules were seen in the MD study leading from $Y288_I$-OH to the binuclear center itself, an observation also consistent with our crystal structure, albeit the exact positions of the water molecules in the two studies are different.

In another model ([18]), the strong hydrogen bond between the $Y288_I$-OH and heme a_3 farnesyl-OH is envisioned to be a gate controlling proton uptake through the K path. In the oxidized enzyme, the average distance between the two OH groups is 2.6 Å in the high resolution crystal structures of bovine and *Rs*C*c*O, indicating that the gate is closed. During the initial reductive phase of the cycle, the covalently crosslinked $Y288_I$/$H284_I$ ligand of Cu_B is proposed to be transiently released from Cu_B, and to undergo a conformational change that weakens the OH-OH hydrogen bond and opens the gate ([18]). In line with this prediction, one could postulate that the trigger for the conformational changes seen in the reduced crystal structure is the rearrangement of the His-Tyr Cu_B ligand, resulting in a loss of the OH-OH bond.

The observed conformational flexibility of helix VIII is also consistent with H/D exchange studies, which identify this region as largely solvent inaccessible in the oxidized state, but becoming solvent accessible in the reduced state ([19]). In addition, computer modeling studies using the ProFlex program ([58]) suggest that this part of helix VIII is a relatively flexible region (Buhrow L. and Kuhn, L., unpublished work).

The coordination between the D path and the K path

H/D exchange studies of *Rs*C*c*O in various intermediate states show little solvent accessibility for the majority of D path residues during the catalytic cycle ([19]). It is therefore perhaps not surprising that the hydrogen bonded water chain connecting $D132_I$ to $E286_I$ is highly stable in many crystal structures, with the exception of mutants that are known to affect proton uptake, such as $D132A_I$ (Liu *et al*, unpublished results). Indeed, we observe no change in the D path water chain between the oxidized and reduced states of the wild type *Rs*C*c*O.

$E286_I$, a key residue in the D path buried in the center of the membrane, was suggested by experimental and modeling studies to undergo conformational changes during the cycle, from a down-position connected to the D path, to an up-position connected to the active site or to the D-propionate region above heme a_3 via newly formed water chains ([11, 59, 60]). This conformational change is suggested to be a D path gate ([61]). None of the crystal structures of C*c*O available so far have revealed the postulated additional water chains in this largely

hydrophobic area. However, in the crystal structure of the two-subunit *Rs*C*c*O in the oxidized state, one water molecule is resolved in a position that could be part of such a chain ([7]) (Figure 4). The position of this additional water molecule is unique: it forms hydrogen bonds with the main chain carbonyl oxygen of $G283_I$, as well as the Cu_B ligand OH^-. Interestingly, this additional water is also within hydrogen bonding distance of the carboxyl oxygen of $E286_I$ when it is in one of its possible up-conformations, making this water a candidate for bridging between the D path and the active site. This water could also connect to a proton exit route, via crystallographically unresolved water molecules. It is seen in a number of high resolution *Rs*C*c*O structures in the oxidized state, including the deoxycholate bound structure (PDB entry 3DTU)([62]), as well as several structures of mutant forms (Liu *et al*, unpublished work).

However, this water disappears completely in the reduced structure, partly because one of its hydrogen bonding ligands, the OH^- bound to Cu_B, is lost from the binuclear center. The disappearance suggests that the D path connection to the binuclear center is disrupted, at the same time as the K path connection is open. This implies a coordinated change in connectivity to the binuclear center with access controlled by the metal chemistry to prevent proton short circuiting between the two pathways.

Other possible explanations for the observed structural changes in the reduced RsCcO

Suicide inactivation is a typical behavior observed in C*c*O lacking subunit III. It is characterized by spontaneous and irreversible loss of activity during catalytic turnover ([37]). The underlying mechanism of suicide inactivation is not entirely understood at present, but it occurs when proton uptake through the D path (but not the K path) is impaired and not compensated for by proton backflow ([63]). As expected, the redissolved I-II subunit *Rs*C*c*O crystal exhibits suicide inactivation during steady state turnover ([7]). It is reasonable to speculate that the observed structural changes in the reduced I-II subunit CcO could represent a form of the enzyme that is already inactivated, or an intermediate en route to inactivation. However, when the reduced crystals are redissolved, they exhibit normal spectrum and oxidase activity (Figure 5). When the reduced crystals were reoxidized with ferricyanide, the displacement of heme a_3 and residue movements in helix VIII returned to normal. Most importantly, these structural changes were also seen in the reduced structure of the four-subunit *Rs*C*c*O, which does not show suicide inactivation. These lines of evidence demonstrate that this structure is not an artifact of the two subunit enzyme. Similarly, as described in Results, the changes in conformation associated with reduction are not due to the inhibitory binding of Cd at the $E101_{II}$ site.

It should also be noted that reduction was carried out on crystals that were formed in the oxidized state. Thus it is possible that the changes seen are restricted by the crystal packing, which may limit the longer distance transmission of conformational effects.

In conclusion the crystal structure of the *Rs*C*c*O in the fully reduced form shows novel structural changes compared to the oxidized form, which could simulate a physiological intermediate during the catalytic cycle. The major changes in the region of heme a_3 and helix VIII have not been reported in reduced structures of C*c*O from other sources, but are consistent with evidence from computational and H/D exchange approaches. The observed changes minimally indicate significant flexibility in the region of heme a_3, and suggest a specific mechanism for gating of the K path and for alternating access to the D and K pathways.

Supplementary Material

Refer to Web version on PubMed Central for supplementary material.

Abbreviations

C*c*O, cytochrome *c* oxidase
Rs, *Rhodobacter sphaeroides*
I–II *Rs*C*c*O, the form of *Rs*C*c*O containing the catalytic core subunits I and II
Pd, *Paracoccus denitrificans*
PDB, Protein Data Bank
ATP, adenosine triphosphate
PEG-400, polyethylene glycol with an average molecular weight of 400
MES, 2-(*N*-morpholino)ethanesulfonic acid
HEPES, 4-(2-Hydroxyethyl)piperazine-1-ethanesulfonic acid
TMPD, *N,N,N′,N′*-tetramethyl-*p*-phenylenediamine
MD, molecular dynamics. Unless otherwise noted, the amino acid numbering of cytochrome *c* oxidase in this article is from *Rhodobacter sphaeroides*, with the subscript representing the subunit number

Acknowledgements

We thank Dr. R. Michael Garavito from the Biochemistry and Molecular Biology Department, Michigan State University, for his support and consultation. We thank beamline staff scientists Zdzislaw Wawrzak, Joseph Brunzelle, Spencer Anderson, and Keith Brister from LS-CAT, Ruslan Sanishvili (Nukri), Michael Becker, Nagarajan Venugopalan, Stephen Corcoran, Derek Yoder, Ward Smith, and Robert Fischetti from GM/CA-CAT, and Vukica Srajer and Yu-Sheng Chen from BioCARS, Advanced Photon Source, Argonne National Laboratory, for their help during data collection. We thank Drs. Martyn A. Sharpe, Peter Nicholls, Steve Seibold and Jonathan P. Hosler for helpful discussions and suggestions.

References

1. Hosler JP, Ferguson-Miller S, Mills DA. Energy transduction: proton transfer through the respiratory complexes. Annu Rev Biochem 2006;75:165–187. [PubMed: 16756489]
2. Brzezinski P, Gennis R. Cytochrome c oxidase: exciting progress and remaining mysteries. J Bioenerg Biomembr 2008;40:521–531. [PubMed: 18975062]
3. Wikstrom M, Verkhovsky MI. Mechanism and energetics of proton translocation by the respiratory heme-copper oxidases. Biochim Biophys Acta 2007;1767:1200–1214. [PubMed: 17689487]
4. Iwata S, Ostermeier C, Ludwig B, Michel H. Structure at 2.8 .ANG. resolution of cytochrome c oxidase from Paracoccus denitrificans. Nature (London) 1995;376:660–669. [PubMed: 7651515]
5. Fetter JR, Qian J, Shapleigh J, Thomas JW, Garcia-Horsman A, Schmidt E, Hosler J, Babcock GT, Gennis RB, Ferguson-Miller S. Possible proton relay pathways in cytochrome c oxidase. Proc Natl Acad Sci U S A 1995;92:1604–1608. [PubMed: 7878026]
6. Svensson-Ek M, Abramson J, Larsson G, Tornroth S, Brzezinski P, Iwata S. The X-ray Crystal Structures of Wild-type and EQ(I-286) Mutant Cytochrome c Oxidases from Rhodobacter sphaeroides. J Mol Biol 2002;321:329–339. [PubMed: 12144789]
7. Qin L, Hiser C, Mulichak A, Garavito RM, Ferguson-Miller S. Identification of conserved lipid/detergent-binding sites in a high-resolution structure of the membrane protein cytochrome c oxidase. Proc Natl Acad Sci U S A 2006;103:16117–16122. [PubMed: 17050688]
8. Konstantinov AA, Siletsky S, Mitchell D, Kaulen A, Gennis RB. The roles of the two proton input channels in cytochrome c oxidase from Rhodobacter sphaeroides probed by the effects of site-directed mutations on time-resolved electrogenic intraprotein proton transfer. Proc Natl Acad Sci U S A 1997;94:9085–9090. [PubMed: 9256439]
9. Adelroth P, Ek MS, Mitchell DM, Gennis RB, Brzezinski P. Glutamate 286 in cytochrome aa3 from Rhodobacter sphaeroides is involved in proton uptake during the reaction of the fully-reduced enzyme with dioxygen. Biochemistry 1997;36:13824–13829. [PubMed: 9374859]
10. Busenlehner LS, Branden G, Namslauer I, Brzezinski P, Armstrong RN. Structural elements involved in proton translocation by cytochrome c oxidase as revealed by backbone amide hydrogen-deuterium exchange of the E286H mutant. Biochemistry 2008;47:73–83. [PubMed: 18052347]

11. Hofacker I, Schulten K. Oxygen and proton pathways in cytochrome c oxidase. Proteins 1998;30:100–107. [PubMed: 9443344]
12. Branden M, Sigurdson H, Namslauer A, Gennis RB, Adelroth P, Brzezinski P. On the role of the K-proton transfer pathway in cytochrome c oxidase. Proc Natl Acad Sci U S A 2001;98:5013–5018. [PubMed: 11296255]
13. Adelroth P, Gennis RB, Brzezinski P. Role of the pathway through K(I-362) in proton transfer in cytochrome c oxidase from R. sphaeroides. Biochemistry 1998;37:2470–2476. [PubMed: 9485395]
14. Branden M, Tomson F, Gennis RB, Brzezinski P. The entry point of the K-proton-transfer pathway in cytochrome c oxidase. Biochemistry 2002;41:10794–10798. [PubMed: 12196018]
15. Richter O-MH, Duerr KL, Kannt A, Ludwig B, Scandurra FM, Giuffre A, Sarti P, Hellwig P. Probing the access of protons to the K pathway in the Paracoccus denitrificans cytochrome c oxidase. FEBS Journal 2005;272:404–412. [PubMed: 15654878]
16. Hosler JP, Shapleigh JP, Mitchell DM, Kim Y, Pressler MA, Georgiou C, Babcock GT, Alben JO, Ferguson-Miller S, Gennis RB. Polar residues in helix VIII of subunit I of cytochrome c oxidase influence the activity and the structure of the active site. Biochemistry 1996;35:10776–10783. [PubMed: 8718868]
17. Sharpe, MA.; Qin, L.; Ferguson-Miller, S. Proton entry, exit and pathways in cytochrome oxidase: Insight from conserved water. In: Wikstrom, M., editor. Biophys. Struct. Aspects Bioenerg. Cambridge, UK: Royal Society of Chemistry; 2005. p. 26-54.
18. Sharpe M, Ferguson-Miller S. A chemically explicit model for the mechanism of proton pumping in heme–copper oxidases. J Bioenerg Biomembr 2008;40:541–549. [PubMed: 18830692]
19. Busenlehner LS, Salomonsson L, Brzezinski P, Armstrong RN. Mapping protein dynamics in catalytic intermediates of the redox-driven proton pump cytochrome c oxidase. Proc Natl Acad Sci U S A 2006;103:15398–15403. [PubMed: 17023543]
20. Zhen Y, Qian J, Follmann K, Hayward T, Nilsson T, Dahn M, Hilmi Y, Hamer AG, Hosler JP, Ferguson-Miller S. Overexpression and purification of cytochrome c oxidase from Rhodobacter sphaeroides. Protein Expr Purif 1998;13:326–336. [PubMed: 9693057]
21. Qin L, Mills DA, Hiser C, Murphree A, Garavito RM, Ferguson-Miller S, Hosler J. Crystallographic Location and Mutational Analysis of Zn and Cd Inhibitory Sites and Role of Lipidic Carboxylates in Rescuing Proton Path Mutants in Cytochrome c Oxidase. Biochemistry 2007;46:6239–6248. [PubMed: 17477548]
22. Otwinowski Z, Minor W. Processing of x-ray diffraction data collected in oscillation mode. Methods in Enzymology 1997;276:307–326.
23. Murshudov GN, Vagin AA, Dodson EJ. Refinement of macromolecular structures by the maximum-likelihood method. Acta Crystallogr D Biol Crystallogr 1997;D53:240–255. [PubMed: 15299926]
24. Bailey S. The CCP4 suite: programs for protein crystallography. Acta Crystallogr D Biol Crystallogr 1994;D50:760–763.
25. Emsley P, Cowtan K. Coot: model-building tools for molecular graphics. Acta Crystallogr D Biol Crystallogr 2004;D60:2126–2132. [PubMed: 15572765]
26. Brunger AT, Adams PD, Clore GM, DeLano WL, Gros P, Grosse-Kunstleve RW, Jiang J-S, Kuszewski J, Nilges M, Pannu NS, Read RJ, Rice LM, Simonson T, Warren GL. Crystallography & NMR System: a new software suite for macromolecular structure determination. Acta Crystallographica, Section D: Biological Crystallography 1998;D54:905–921.
27. Pearson AR, Pahl R, Kovaleva EG, Davidson VL, Wilmot CM. Tracking X-ray-derived redox changes in crystals of a methylamine dehydrogenase/amicyanin complex using single-crystal UV/Vis microspectrophotometry. J Synchrotron Radiat 2007;14:92–98. [PubMed: 17211075]
28. Harrenga A, Michel H. The cytochrome c oxidase from Paracoccus denitrificans does not change the metal center ligation upon reduction. J Biol Chem 1999;274:33296–33299. [PubMed: 10559205]
29. Yoshikawa S, Shinzawa-itoh K, Nakashima R, Yaono R, Yamashita E, Inoue N, Yao M, Fei MJ, Libeu CP, Mizushima T, Yamaguchi H, Tomizaki T, Tsukihara T. Redox-coupled crystal structural changes in bovine heart cytochrome c oxidase. Science (Washington, D. C.) 1998;280:1723–1729.
30. Liu B, Chen Y, Doukov T, Soltis SM, Stout CD, Fee JA. Combined microspectrophotometric and crystallographic examination of chemically-reduced and X-ray radiation-reduced forms of

chtochrome ba3 oxidase from Thermus thermophilus: structure of the reduced form of the enzyme. Biochemistry 2009;48:820–826. [PubMed: 19140675]

31. Van Steelandt-Frentrup J, Salmeen I, Babcock GT. A ferrous, high-spin heme a model for cytochrome a3 in the dioxygen reducing site of cytochrome oxidase. J Am Chem Soc 1981;103:5981–5982.
32. Petersen LC. The effect of inhibitors on the oxygen kinetics of cytochrome c oxidase. Biochim Biophys Acta 1977;460:299–307. [PubMed: 192290]
33. van Buuren KJ, Nicholls P, van Gelder BF. Biochemical and biophysical studies on cytochrome aa 3. VI. Reaction of cyanide with oxidized and reduced enzyme. Biochim Biophys Acta 1972;256:258–276.
34. Rich PR, Breton J. FTIR Studies of the CO and Cyanide Adducts of Fully Reduced Bovine Cytochrome c Oxidase. Biochemistry 2001;40:6441–6449. [PubMed: 11371207]
35. Mills DA, Schmidt B, Hiser C, Westley E, Ferguson-Miller S. Membrane potential-controlled inhibition of cytochrome c oxidase by zinc. J Biol Chem 2002;277:14894–14901. [PubMed: 11832490]
36. Aagaard A, Namslauer A, Brzezinski P. Inhibition of proton transfer in cytochrome c oxidase by zinc ions: delayed proton uptake during oxygen reduction. Biochim Biophys Acta 2002;1555:133–139. [PubMed: 12206905]
37. Bratton MR, Pressler MA, Hosler JP. Suicide Inactivation of Cytochrome c Oxidase: Catalytic Turnover in the Absence of Subunit III Alters the Active Site. Biochemistry 1999;38:16236–16245. [PubMed: 10587446]
38. Tsukihara T, Shimokata K, Katayama Y, Shimada H, Muramoto K, Aoyama H, Mochizuki M, Shinzawa-itoh K, Yamashita E, Yao M, Ishimura Y, Yoshikawa S. The low-spin heme of cytochrome c oxidase as the driving element of the proton-pumping process. Proc Natl Acad Sci U S A 2003;100:15304–15309. [PubMed: 14673090]
39. Behr J, Hellwig P, Mantele W, Michel H. Redox dependent changes at the heme propionates in cytochrome c oxidase from Paracoccus denitrificans: direct evidence from FTIR difference spectroscopy in combination with heme propionate 13C labeling. Biochemistry 1998;37:7400–7406. [PubMed: 9585554]
40. Wikstrom M, Verkhovsky MI, Hummer G. Water-gated mechanism of proton translocation by cytochrome c oxidase. Biochimica et Biophysica Acta 2003;1604:61–65. [PubMed: 12765763]
41. Quenneville J, Popovic DM, Stuchebrukhov AA. Redox-Dependent pKa of CuB Histidine Ligand in Cytochrome c Oxidase. J. Phys. Chem. B 2004;108:18383–18389.
42. Ciaccio C, Coletta A, De Sanctis G, Marini S, Coletta M. Cooperativity and allostery in hemoglobin function. IUBMB Life 2008;60:112–123. [PubMed: 18380000]
43. Nurizzo D, Cutruzzola F, Arese M, Bourgeois D, Brunori M, Cambillau C, Tegoni M. Does the reduction of c heme trigger the conformational change of crystalline nitrite reductase? J Biol Chem 1999;274:14997–15004. [PubMed: 10329702]
44. Williams PA, Fulop V, Garman EF, Saunders NF, Ferguson SJ, Hajdu J. Haem-ligand switching during catalysis in crystals of a nitrogen-cycle enzyme. Nature 1997;389:406–412. [PubMed: 9311786]
45. Yoshikawa, S. Structural chemical studies on the reaction mechanism of cytochrome c oxidase. In: Wikstrom, M., editor. Biophys. Struct. Aspects Bioenerg. Cambridge, UK: Royal Society of Chemistry; 2005. p. 55-71.
46. Zickermann I, Tautu OS, Link TA, Korn M, Ludwig B, Richter OM. Expression studies on the ba3 quinol oxidase from Paracoccus denitrificans. A bb3 variant is enzymatically inactive. Eur J Biochem 1997;246:618–624. [PubMed: 9219517]
47. Saiki K, Mogi T, Anraku Y. Heme O biosynthesis in Escherichia coli: the cyoE gene in the cytochrome bo operon encodes a protoheme IX farnesyltransferase. Biochem Biophys Res Commun 1992;189:1491–1497. [PubMed: 1336371]
48. Contreras-Zentella M, Mendoza G, Membrillo-Hernandez J, Escamilla JE. A novel double heme substitution produces a functional bo3 variant of the quinol oxidase aa3 of Bacillus cereus. Purification and paratial characterization. J Biol Chem 2003;278:31473–31478.

49. Shimokata K, Katayama Y, Murayama H, Suematsu M, Tsukihara T, Muramoto K, Aoyama H, Yoshikawa S, Shimada H. The proton pumping pathway of bovine heart cytochrome c oxidase. Proc Natl Acad Sci U S A 2007;104:4200–4205. [PubMed: 17360500]
50. Lee, H-m; Das, TK.; Rousseau, DL.; Mills, D.; Ferguson-Miller, S.; Gennis, RB. Mutations in the Putative H-Channel in the Cytochrome c Oxidase from Rhodobacter sphaeroides Show That This Channel Is Not Important for Proton Conduction but Reveal Modulation of the Properties of Heme a. Biochemistry 2000;39:2989–2996. [PubMed: 10715119]
51. Bae E, Phillips GN Jr. Structures and analysis of highly homologous psychrophilic, mesophilic, and thermophilic adenylate kinases. J Biol Chem 2004;279:28202–28208. [PubMed: 15100224]
52. Sanishvili R, Volz KW, Westbrook EM, Margoliash E. The low ionic strength crystal structure of horse cytochrome c at 2.1 A resolution and comparison with its high ionic strength counterpart. Structure 1995;3:707–716. [PubMed: 8591047]
53. Takano T, Dickerson RE. Conformation change of cytochrome c. II. Ferricytochrome c refinement at 1.8 A and comparison with the ferrocytochrome structure. J Mol Biol 1981;153:95–115. [PubMed: 6279868]
54. Smirnova I, Zaslavsky D, Fee J, Gennis R, Brzezinski P. Electron and proton transfer in the ba 3 oxidase from Thermus thermophilus. Journal of Bioenergetics and Biomembranes 2008;40:281–287. [PubMed: 18752061]
55. Pecoraro C, Gennis RB, Vygodina TV, Konstantinov AA. Role of the K-channel in the pH-dependence of the reaction of cytochrome c oxidase with hydrogen peroxide. Biochemistry 2001;40:9695–9708. [PubMed: 11583170]
56. Brzezinski P, Adelroth P. Pathways of proton transfer in cytochrome c oxidase. J Bioenerg Biomembr 1998;30:99–107. [PubMed: 9623811]
57. Cukier RI. A molecular dynamics study of water chain formation in the proton-conducting K channel of cytochrome c oxidase. Biochim Biophys Acta 2005;1706:134–146. [PubMed: 15620374]
58. Jacobs DJ, Rader AJ, Kuhn LA, Thorpe MF. Protein flexibility predictions using graph theory. Proteins 2001;44:150–165. [PubMed: 11391777]
59. Puustinen A, Wikstrom M. Proton exit from the heme-copper oxidase of Escherichia coli. Proc Natl Acad Sci U S A 1999;96:35–37. [PubMed: 9874767]
60. Seibold SA, Mills DA, Ferguson-Miller S, Cukier RI. Water chain formation and possible proton pumping routes in Rhodobacter sphaeroides cytochrome c oxidase: a molecular dynamics comparison of the wild type and R481K mutant. Biochemistry 2005;44:10475–10485. [PubMed: 16060656]
61. Kaila VR, Verkhovsky MI, Hummer G, Wikstrom M. Glutamic acid 242 is a valve in the proton pump of cytochrome c oxidase. Proc Natl Acad Sci U S A 2008;105:6255–6259. [PubMed: 18430799]
62. Qin L, Mills DA, Buhrow L, Hiser C, Ferguson-Miller S. A conserved steroid binding site in cytochrome C oxidase. Biochemistry 2008;47:9931–9933. [PubMed: 18759498]
63. Mills DA, Tan Z, Ferguson-Miller S, Hosler J. A role for subunit III in proton uptake into the D pathway and a possible proton exit pathway in Rhodobacter sphaeroides cytochrome c oxidase. Biochemistry 2003;42:7410–7417. [PubMed: 12809496]

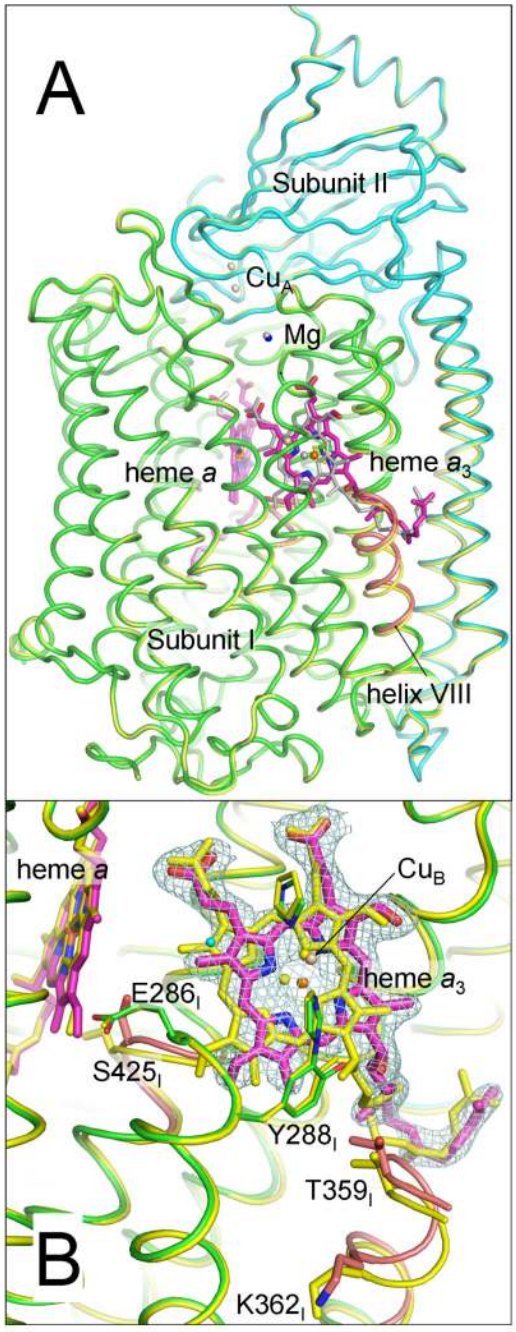

Figure 1.

Comparison of *Rs*C*c*O structure between the reduced and oxidized states. (A). Overall structure of I-II subunit *Rs*C*c*O. In the reduced structure, the protein backbone is displayed in cartoon and colored by different subunits (subunit I: green; subunit II: cyan), and the heme groups, *a* and a_3, are shown in sticks and colored by atom type (C: magenta; O: red; N: blue). The metals in the reduced structure are displayed in spheres and colored differently (Fe: orange; Cu: wheat; Mg: blue). In the oxidized structure, the protein subunits are colored yellow, and the heme groups and metals are colored gray. Two patches of peptides in the reduced structure, where significant conformational changes are observed compared with those in the oxidized structure, are shown in deep salmon. (B). Structure at the active site region. The reduced structure is

colored in the same manner as in (A), while that of the oxidized structure is colored yellow. The ($2F_o$-F_c) difference Fourier map contoured at 1.0 σ level is colored light blue. Several key residues in the structures are displayed in sticks, and colored by atom type in the reduced structure and yellow in the oxidized structure.

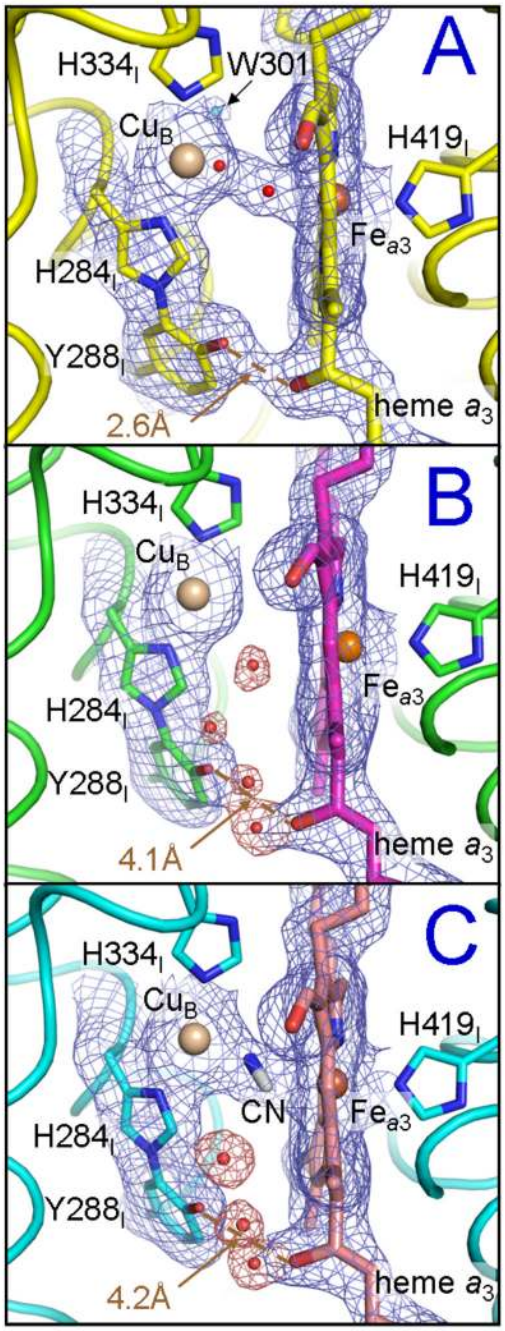

Figure 2.

Structural comparison of the active site in the oxidized (A), reduced (B) and cyanide-bound reduced (C) states of *Rs*C*c*O. (A). In the oxidized structure, the protein backbone is colored yellow, heme a_3 and several key residues in the active site region are displayed as sticks and colored by atom type (C: yellow; O: red, N: blue). The metals Fe-a_3 and Cu_B are displayed as spheres and colored orange and wheat, respectively. The two bridging ligands between Cu_B and Fe-a_3, temporarily assigned as an OH^- ligated to Cu_B and a water ligated to Fe, are displayed as small red spheres. The water molecule (W301) resolved in the hydrophobic region near the binuclear center between the top of the D path and the binuclear center is displayed as a cyan sphere. ($2F_o$-F_c) difference Fourier map contoured at 1.0 σ is colored blue. (B). In

the reduced structure, the protein backbone is colored green, several key residues in the active site region is colored by atom type (C: green; O: red; N: blue), and heme a_3 is colored by a different color scheme (C: magenta; O: red; N: blue). The metals are displayed in the same manner as in (A), and additionally resolved water molecules in the reduced structure are displayed in small red spheres. ($2F_o$-F_c) difference Fourier map surrounding the binuclear center, contoured at 1.0 σ, is colored blue; and that surrounding the additionally resolved water molecules is colored red. (C). In the cyanide-bound reduced structure, the protein backbone is colored cyan, several key residues in the active site region is colored by atom type (C: cyan; O: red; N: blue), and heme a_3 is colored by a different color scheme (C: salmon; O: red; N: blue). The metals and additionally resolved water molecules in the reduced structure are displayed in the same manner as in (B). The cyanide molecule is displayed as sticks and colored by atom type (C: gray; N: blue). ($2F_o$-F_c) difference Fourier map is displayed in the same manner as in (B). In all structures, the O-O distance between the $Y288_I$-OH and the OH group of the heme a_3 hydroxyl farnesyl tail is represented by the brown dashed line and labeled.

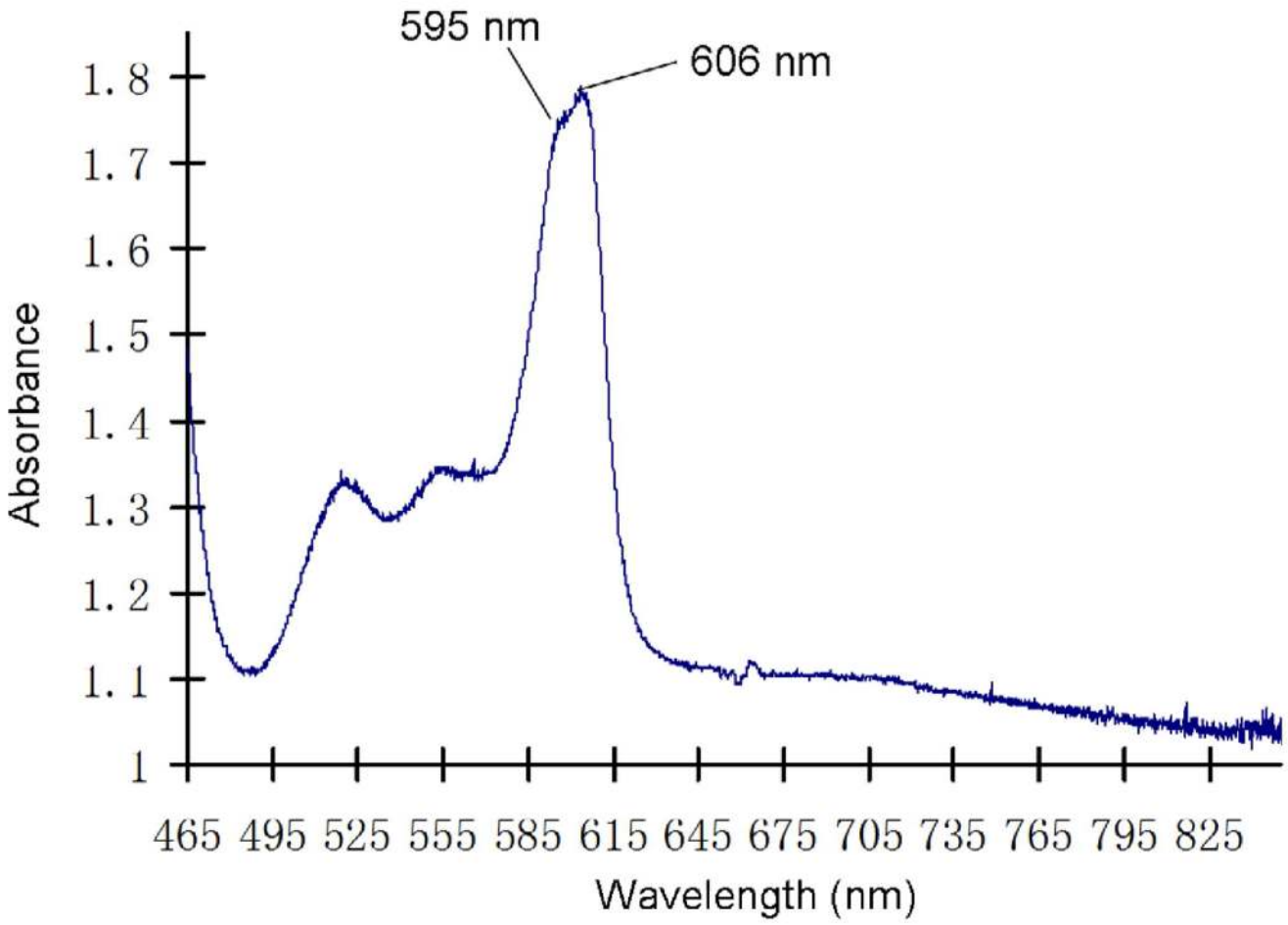

Figure 3.
Spectrum of CN-bound reduced *Rs*C*c*O crystal. The spectrum was taken of the frozen crystal before irradiation at 100K at beamline 14-BM-C, BioCARS, Advanced Photon Source as described in Materials and Methods.

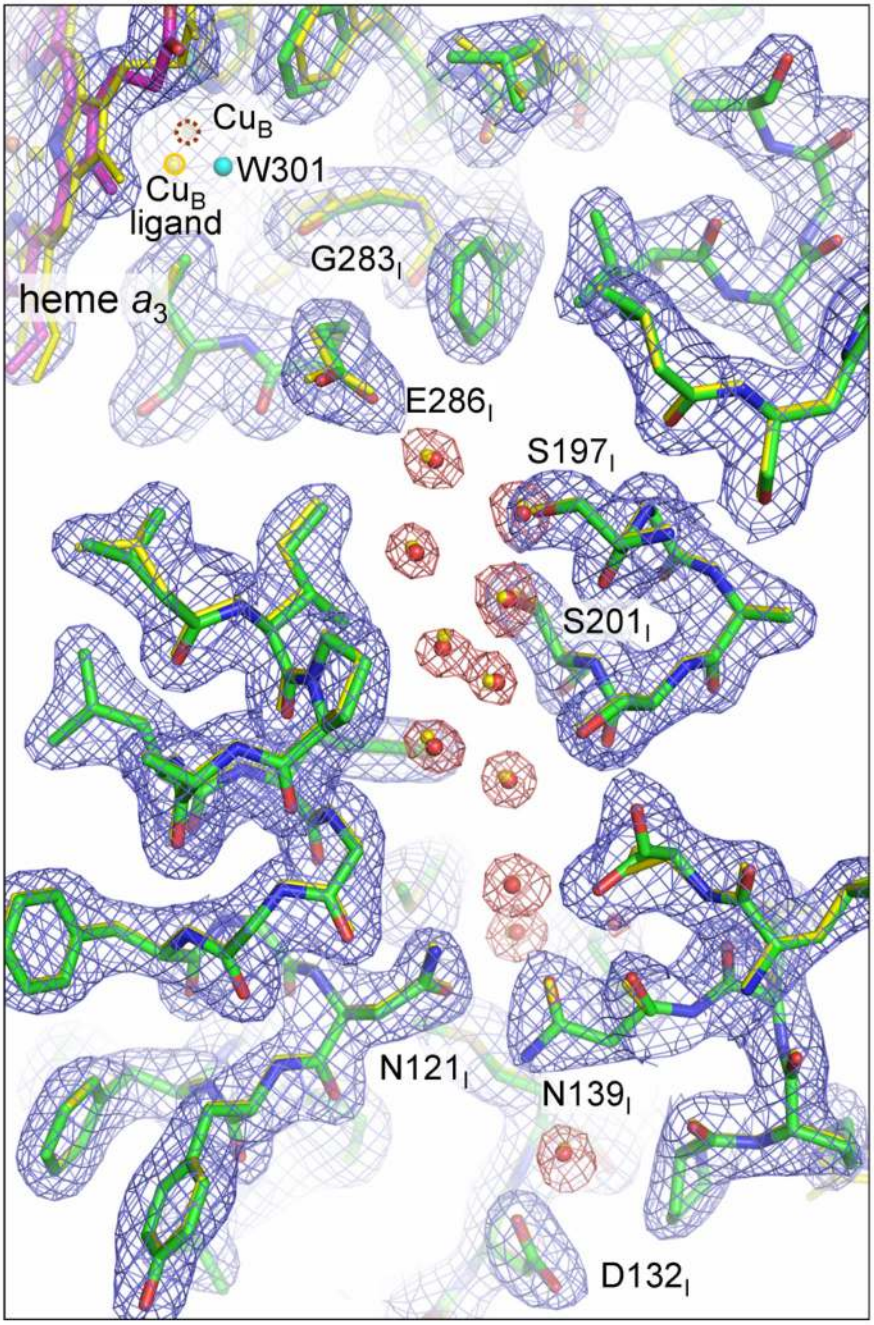

Figure 4.

Comparison of the reduced vs. oxidized structures in the D path. In the reduced structure, the amino acid residues are displayed in sticks and colored by atom type (C: green; O: red, N: blue), and heme a_3 also displayed as sticks and colored by atom type (C: magenta; O: red; N: blue). Water molecules resolved in the D path are displayed as small red spheres. In this view, the Cu_B center is deep in the background and hardly visible, and its presence is highlighted by a brown dashed circle. ($2F_o$-F_c) difference Fourier electron density map, contoured at 1.0 σ, is colored dark red for regions surrounding the D path waters, and blue for everywhere else. The oxidized structure is displayed in the same style as in the reduced structure and is colored yellow, except that the extra water (W301) resolved between the top of the D path and the

binuclear center is shown as a cyan sphere. One of the ligands of W301 in the oxidized structure, temporarily assigned as an OH^- ligated to Cu_B, is not clearly visible in this view and its presence is highlighted by a yellow circle and is labeled as Cu_B ligand in the figure.

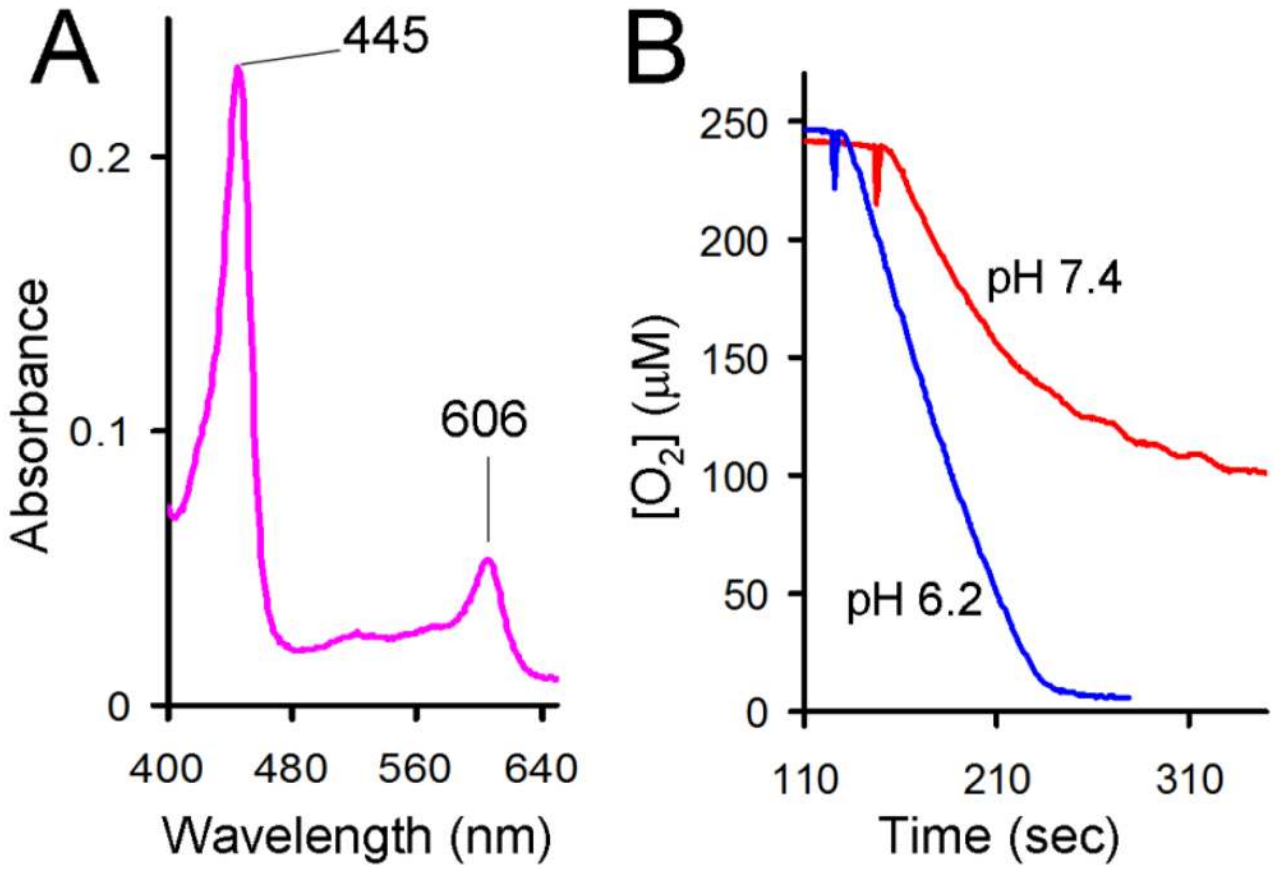

Figure 5.

(A). Optical spectrum of redissolved reduced crystals of I-II *Rs*C*c*O. The spectrum is obtained by dissolving previously reduced crystals in buffer with added dithionite, showing native C*c*O characteristics. (B). Activity assays of redissolved reduced I-II *Rs*C*c*O crystals. Suicide inactivation of C*c*O is observed at pH 7.4 (red trace), with an initial velocity of 1067 e^-/sec; this suicide inactivation is alleviated by lowering pH (pH 6.2, blue trace), with an initial velocity of 1680 e^-/sec.

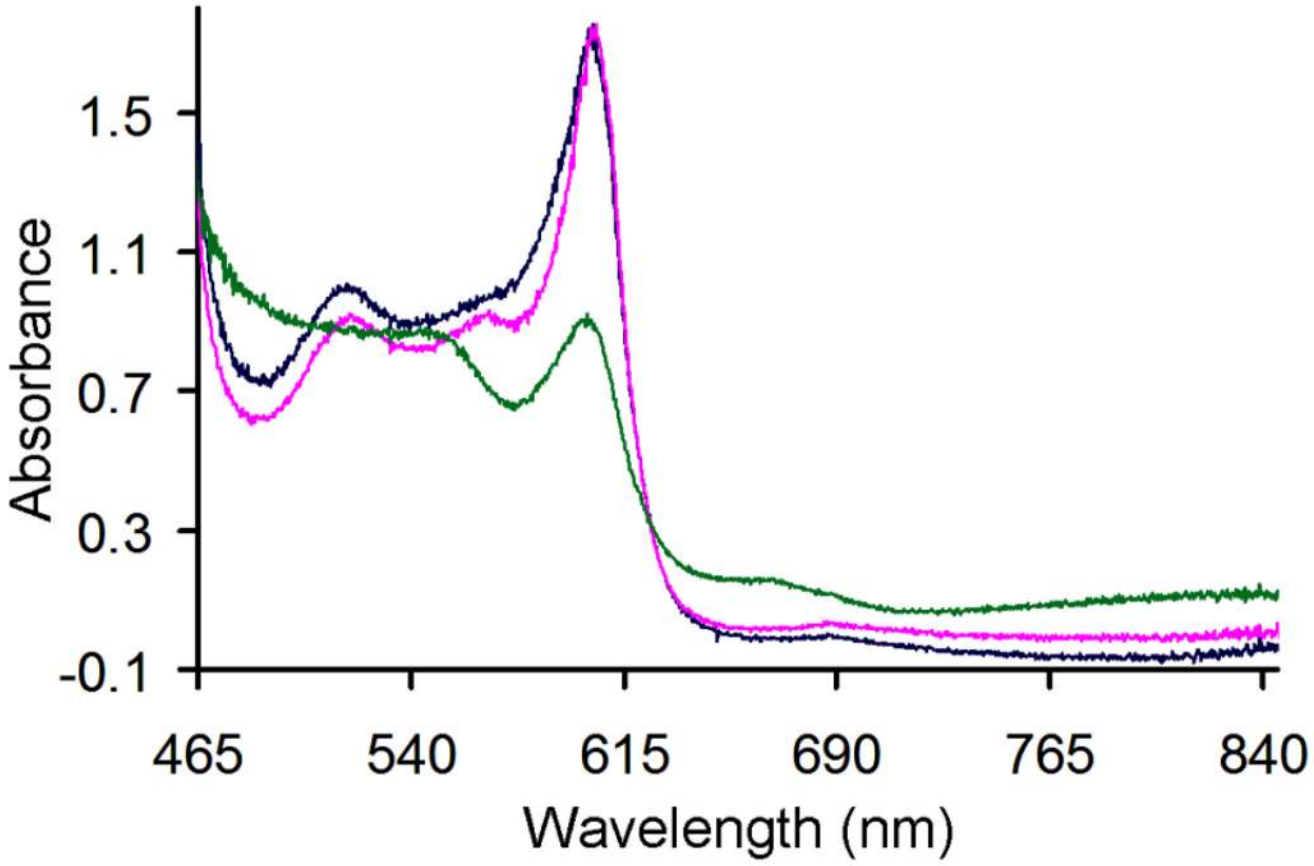

Figure 6.

Spectral studies of irradiated reduced crystals. The blue spectrum was taken immediately after the irradiated, reduced crystal was transferred from liquid nitrogen into the soaking buffer that contained a small amount of dithionite to remove oxygen and prevent oxidation. The magenta spectrum was taken approximately two minutes after the crystal was soaked in the cryosolution supplemented with dithionite. The dark green spectrum was taken approximately 10 minutes after the soaking buffer was exchanged into fresh oxygenated buffer. The spectra that were recorded show normal characteristics of the native enzyme.

Table 1

Data collection and refinement statistics of reduced and cyanide-bound reduced *Rs*C*c*O.

	Dithionite reduced	Cyanide-bound dithionite reduced
A. Unit Cell Parameters		
Space Group	$P\ 2_12_12_1$	$P\ 2_12_12_1$
Cell dimensions (Å)	*a*=124.6 *b*=131.5 *c*=176.2	*a*=124.3 *b*=131.9 *c*=176.2
Molecules per asym. unit	2	2
B. Data Collection		
Resolution range (Å)	50 – 2.15 (2.15 – 2.206)[a]	50 – 2.2 (2.20 – 2.257) [a]
Completeness (%)	99.1 (92.7) [a]	96.2 (73.5) [a]
No. of unique reflections	151,414 (10,311) [a]	137,425 (7,652) [a]
Redundancy	4.6 (4.0) [a]	6.7 (3.7) [a]
Rmerge (%)	6.5 (60.6) [a]	7.2 (52.0) [a]
I / σ	20.8 (1.8) [a]	20.3 (1.9) [a]
C. Structural Refinement		
No. of refined atoms	13615	13605
R-factor / R free (%)	19.6 / 22.1 (27.4 / 29.5) [a]	19.4 / 21.9 (25.5 / 30.1) [a]
Average B-factor	45.8	44.0
R.m.s.d. bond length (Å)	0.012	0.011
R.m.s.d bond angle (°)	1.227	1.155

Rmerge = $\sum | Ih - \langle Ih \rangle | / \sum Ih$ over all *h*, where *Ih* is the intensity of reflection *h*.

R-factor= $\sum | |Fo| - |Fc| | / \sum |Fo|$; where *F*o and *F*c are the observed and calculated structure factors, respectively. A randomly selected subset of the data (3%, approximately 4000 reflections) was used to calculate R_{free}

[a] highest resolution shell